

VIP

SPECIAL
ISSUE

Syntheses, Structures and Sorption Properties of Three Isorecticular Trinuclear Indium-Based Amide-Functionalized Metal–Organic Frameworks

Zong-Hui Zhang,^[a] Qian Wang,^[a] Dong-Xu Xue,^{*,[a]} and Junfeng Bai^{*,[a, b]}

Abstract: Amide-functionalized metal–organic frameworks (AFMOFs) as a subclass of MOF materials have received great interest recently because of their intriguing structures and diverse potential applications. In this work, solvothermal reactions between indium nitrate and two mixed-linkers afforded two new isorecticular 8-connected trinuclear indium-based AFMOFs of $[(\text{In}_3\text{O})(\text{OH})(\text{L}_2)_2(\text{IN})_2]\cdot(\text{solv})_x$ (**2-In**) and $[(\text{In}_3\text{O})(\text{OH})(\text{L}_2)_2(\text{AIN})_2]\cdot(\text{solv})_x$ (**NH₂-2-In**) ($\text{H}_2\text{L}_2 = 4,4'$ -(carbonylimino)dibenzoic acid and HIN = isonicotinic acid or HAIN = 3-aminoisonicotinic acid), respectively. Moreover, by means of reticular chemistry, an extended network of $[(\text{In}_3\text{O})(\text{OH})(\text{L}_3)_2(\text{PB})_2]\cdot(\text{solv})_x$ (**3-In**) ($\text{H}_2\text{L}_3 = 4,4'$ -(terephthaloylbis(azanediyl)dibenzoic acid, HPB = 4-(4-pyridyl)benzoic acid) was also successfully realized after prolongation of the former dicarboxylate linker and HIN, resulting in a truly 8-

connected isorecticular AFMOF platform. These frameworks were structurally determined by single-crystal X-ray diffraction (SCXRD). Sorption studies further demonstrate that **2-In** and **NH₂-2-In** exhibit not only high surface areas and pore volumes but also relatively high carbon capture capabilities (the CO₂ uptakes reach 60.0 and 75.5 cm³ g⁻¹ at 298 K and 760 torr, respectively) due to the presences of amide and/or amine functional groups. The selectivity of CO₂/N₂ and CO₂/CH₄ calculated by IAST are 10.18 and 12.43, 4.20 and 4.23 for **2-In** and **NH₂-2-In**, respectively, which were additionally evaluated by mixed-gases dynamic breakthrough experiments. In addition, high-pressure gas sorption measurements show that both materials could take up moderate amounts of natural gas.

Introduction

Functionalization of metal–organic frameworks (MOFs) is of *para* importance in MOF chemistry to realize/enhance relevant targeting properties. Generally, there are two approaches to generate functional MOFs, including direct synthesis via utilization of pre-functionalized organic linkers^[1] or indirect synthesis, i.e., the so-called post-synthetic modification.^[2] However, newly formed MOF materials by means of above strategies always exhibit improved performances accompanied by much lower surface areas and pore volume. The emerging amide-functionalized MOFs (AFMOFs) as a subclass of MOF materials have attracted more and more attentions recently due to their intrin-

sic structural attributes (built-in amide-functional groups without sacrificing porosities and properties) and prominent achievements toward carbon capture, methane storage and safe handling of acetylene et al.^[3]

The exploration and development of AFMOFs have been initiated in our research group since a decade ago. A fruitful AFMOF library has been designed and constructed ranging from flexible to robust ones based on judicious organic linkers and mainly transitional metal ions.^[4] To extend the scope of AFMOF inventory, it is necessary to choose non-transitional metal ions to target new type ones for specific applications. Indium metal ion as a *p*-block metal element is an interesting central metal to construct MOF materials due to its relatively well-defined molecular building blocks (MBBs) encompassing linear neutral $[\text{In}(\mu\text{-OH})(\text{O}_2\text{C})_2]_2$,^[5] charged trimeric $[\text{In}_3(\mu_3\text{-O})(\text{O}_2\text{C})_6]$ ^[6] and tetrahedral $[\text{In}(\text{O}_2\text{C})_4]/[\text{InN}_4(\text{O}_2\text{C})_4]$,^[7] respectively.

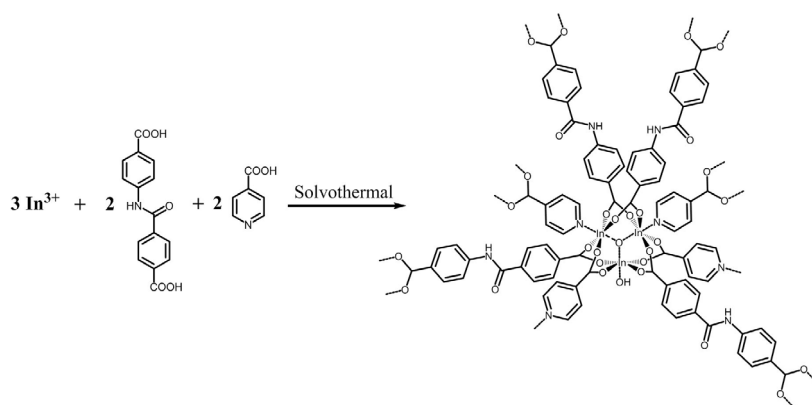
Additionally, multivariate MOFs (MTV-MOFs)^[8] with multiple functional groups pioneered by Yaghi's group have aroused extensive investigations recently to access materials with increased complexity and advanced functions. For instance, a series of MTV-MOFs have been elaborately prepared and detailedly elucidated. A member of MTV-MOF-5-EHI exhibits up to 400% better selectivity for carbon dioxide over carbon monoxide compared with its best same-link counterparts. In contrast to complex characterizations for mentioned MTV-MOFs, mixed-linker strategies may provide another avenue to obtain multi-functional crystalline framework materials along with ease

[a] Dr. Z.-H. Zhang, Dr. Q. Wang, Prof. Dr. D.-X. Xue, Prof. Dr. J. Bai
Key Laboratory of Applied Surface and Colloid Chemistry
Ministry of Education
School of Chemistry & Chemical Engineering
Normal University
Shaanxi, Xi'an 710062 (China)
E-mail: xuedx@snnu.edu.cn
bjunfeng@nju.edu.cn

[b] Prof. Dr. J. Bai
State Key Laboratory of Coordination Chemistry
Nanjing University
Nanjing 210093 (P. R. China)

 Supporting information and the ORCID identification number(s) for the author(s) of this article can be found under:
<https://doi.org/10.1002/asia.201900536>.

 This manuscript is part of a special issue on Metal–Organic Frameworks. A link to the Table of Contents of the special issue will appear here when the complete issue is published.



Scheme 1. Construction Scheme of the uninodal, 8-connected network of **2-In** by mixed linear organic ligands and the μ_3 -O-centered trinuclear Indium cluster.

preparation and unambiguous structural information to correlate the relationship between structure and property.^[9]

Bearing above mentioned in mind, herein, we adopted mixed-linker strategy and indium nitrate as metal source, both isorecticular 8-connected trinuclear indium-based AFMOFs of $[(\text{In}_3\text{O})(\text{OH})(\text{L}2)_2(\text{IN})_2] \cdot (\text{sol}v)_x$ (**2-In**) and $[(\text{In}_3\text{O})(\text{OH})(\text{L}2)_2(\text{AIN})_2] \cdot (\text{sol}v)_x$ (**NH₂-2-In**) ($\text{H}_2\text{L}2 = 4,4'$ -(carbonylimino)dibenzoic acid and HIN = isonicotinic acid or HAIN = 3-aminoisonicotinic acid) were solvothermally isolated (Scheme 1). Moreover, extended network of $[(\text{In}_3\text{O})(\text{OH})(\text{L}3)_2(\text{PB})_2] \cdot (\text{sol}v)_x$ (**3-In**) ($\text{H}_2\text{L}3 = 4, 4'$ -(terephthaloylbis(azanediy))dibenzoic acid, HPB = 4-(4-pyridyl)benzoic acid) was also successfully generated via reticular chemistry^[10] after prolongation of previous dicarboxylate linker and HIN, resulting in a truly new 8-connected AFMOF platform. Sorption studies indicate that **2-In** and **NH₂-2-In** exhibit not only high surface areas and pore volume, but also relatively high carbon capture capabilities due to the presences of amide and/or amine functional groups. In addition, both materials could uptake moderate amounts of natural gas.

Results and Discussion

Synthesis and crystal structures

The MBB of $[\text{M}_3(\mu_3\text{-O})(\text{O}_2\text{C-})_6\text{L}_3]$ ($\text{M} = \text{Cr, Fe, In, et al.}$) is a popular trinuclear metal cluster serving as trigonal prismatic secondary building unit (SBU) for deliberately assembling well-known 6-connected MOFs, i.e., **MIL-101**,^[11] **MIL-88**^[12] and **soc-MOFs** series^[13] via substitution of the available carboxylate groups. Meanwhile, the terminal L sites of the cluster can be also ligated by bridging linear monodentate ligands or triangular monodentate ligands to furnish higher-connected nodes, for instance, the 9-connected **MCF-19**^[14] and **CPM-83**,^[15] respectively. In view of this, we curiously speculate that lower connected new frameworks are possibly to be isolated while reacting appropriate amount/ratio of dicarboxylate

and pyridyl monocarboxylate. Indeed, solvothermal reactions between $\text{In}(\text{NO}_3)_3 \cdot 4.5\text{H}_2\text{O}$ and amide-functionalized dicarboxylate ligand **L2** as well as pyridyl ligands of HIN or HAIN, both new AFMOFs of **2-In** and **NH₂-2-In** were successfully obtained.

SCXRD analysis reveals that both **2-In** and **NH₂-2-In** are isorecticular 8-connected trinuclear indium-based AFMOFs. The crystallographic data and refinement parameters are listed in

Table 1. Crystallographic Data and Structure Refinement Summary for **2-In**, **NH₂-2-In** and **3-In**.

MOFs	2-In	NH₂-2-In	3-In
CCDC number	1910435	1910436	1910437
Formula	$\text{C}_{42}\text{H}_{26}\text{In}_3\text{N}_4\text{O}_{16}$	$\text{C}_{42}\text{H}_{28}\text{In}_3\text{N}_6\text{O}_{16}$	$\text{C}_{240}\text{In}_{12}\text{N}_{24}\text{O}_{72}$
FW	1187.13	1217.16	5748.61
T (K)	153.02	153.0	153.0
Space group	<i>I</i> -43 <i>d</i>	<i>I</i> -43 <i>d</i>	<i>I</i> -43 <i>d</i>
<i>a</i> (Å)	38.127(6)	38.0479(6)	51.057(2)
<i>V</i> (Å ³)	55426(24)	55080(3)	133099(16)
Z	24	24	6
<i>D_c</i> (g cm ⁻³)	0.854	0.881	0.430
μ (mm ⁻¹)	6.250	6.305	2.649
<i>F</i> (000)	13944	14328	16699
Crystal size (mm ³)	0.1 × 0.1 × 0.1	0.1 × 0.1 × 0.1	0.08 × 0.08 × 0.08
θ range for data collection (deg.)	3.666 to 50.346	3.285 to 54.288	2.737 to 51.143
Limiting indices	$-37 < h < 22,$ $-33 < k < 32,$ $-25 < l < 38$	$-40 < h < 14,$ $-17 < k < 37,$ $-25 < l < 33$	$-45 < h < 37,$ $-46 < k < 44,$ $-45 < l < 51$
Reflection collected	19480 [<i>R_{int}</i> = 0.0476]	32306 [<i>R_{int}</i> = 0.0406]	61628 [<i>R_{int}</i> = 0.0299]
Completeness	98.9%	98.9%	99.5%
Data/restraints/parameters	4744/ 2/ 161	5477/ 7/ 200	11671/ 0/ 291
GOF	1.111	1.131	0.985
Final <i>R</i> indices (<i>I</i> > 2σ(<i>I</i>))	<i>R</i> ₁ = 0.0712, <i>wR</i> ₂ = 0.2036	<i>R</i> ₁ = 0.0565, <i>wR</i> ₂ = 0.1595	<i>R</i> ₁ = 0.0977, <i>wR</i> ₂ = 0.2834
<i>R</i> indices (all data)	<i>R</i> ₁ = 0.0729, <i>wR</i> ₂ = 0.2072	<i>R</i> ₁ = 0.0579, <i>wR</i> ₂ = 0.1615	<i>R</i> ₁ = 0.0981, <i>wR</i> ₂ = 0.2837
Largest diff. peak and hole	1.308 and -1.574 e Å ⁻³	1.346 and -0.706 e Å ⁻³	0.83 and -0.88 e Å ⁻³
[^a] $R_1 = \sum F_o - F_c / F_o $; $wR_2 = [\sum w(F_o^2 - F_c^2)^2 / \sum w(F_o^2)^2]^{1/2}$.			

Table 1. For the sake of brevity, only the structure of **2-In** is depicted. **2-In** crystallizes in cubic space group *I-43d* and there are two crystallographically independent, six-coordinated indium ions in the asymmetric unit (Figures S1). Both In^{3+} ions are surrounded by four carboxylate oxygen atoms, one $\mu_3\text{-O}$ atom and pyridyl nitrogen or hydroxyl occupying the sixth site, respectively, resulting in the formation of $[\text{In}_3(\mu_3\text{-O})(\text{O}_2\text{C-})_6(\text{OH})\text{N}_2]$ MBBs (Figure 1a), which is also present in the structures reported by Xu and co-workers.^[16] Each trinuclear indium MBB is bridged through four deprotonated L^{2-} and four deprotonated IN^- linkers to produce a 3D-periodic network (Figure 1b). Topologically, the $[\text{In}_3(\mu_3\text{-O})(\text{O}_2\text{C-})_6(\text{OH})\text{N}_2]$ cluster can be simplified as a node and organic linkers as spacers, subsequently an eight-connected uninodal net with a Schalfli symbol of $(3^2\cdot 4^{17}\cdot 5^6\cdot 6^3)$ is generated (Figure 1b and Figure S5). Due to the different lengths of the dicarboxylate ligand and the nitrogen-based ligand in **2-In**, four types of pores with irregular shape and distinct size are formed (Figure 1c and S4). Fur-

thermore, as the presence of the unconnected third apical position for the trinuclear indium MBB, **2-In** provides higher porosity toward guest uptake capabilities.

It must be mentioned that the extended **3-In** was fortunately achieved after prolongation the dicarboxylate and pyridyl monocarboxylate in **2-In** with bis-amide functionalized organic ligand **L3** and four nitrogen-based organic ligand **PB**, respectively (Figures 1 and S6). Topology analysis shows that **3-In** is the exactly same topology with **2-In** and **NH₂-2-In**, exemplifying a new truly eight-connected isorecticular AFMOF platform via reticular chemistry.

Sorption and carbon capture properties

To address sorption properties, the phase purity of prepared material must be primarily verified. The phase purity of the bulk crystalline materials for **2-In** and **NH₂-2-In** was independently confirmed by similarities between the simulated and as-synthesized powder X-ray diffraction (PXRD) patterns (Figure S7). Moreover, the corresponding solvent accessible free volumes for **2-In** and **NH₂-2-In** were estimated to be 71.6% and 66.9%, respectively, by summing voxels more than 1.2 Å away from the framework using PLATON software.

Gas sorption studies performed on the respective acetone-exchanged **2-In** and acetone-hexane-exchanged **NH₂-2-In** (Figures 2) samples show fully reversible Type-I isotherms, representative of microporous materials. The apparent BET surface area and pore volume for **2-In** and **NH₂-2-In** were estimated to be $2080\text{ m}^2\text{g}^{-1}$, $0.84\text{ cm}^3\text{g}^{-1}$ and $1902\text{ m}^2\text{g}^{-1}$ and $0.76\text{ cm}^3\text{g}^{-1}$, respectively. As shown in Figure S10, the pore-size distributions display four-types of cages, which is in great agreement with the single-crystal structure determination. Clearly, the introduction of amino functional groups in the ligands slightly decreases the pore sizes and surface areas of the resulting MOF of **NH₂-2-In**.

Considering the high porosity and functionality of both MOFs, the variable-temperature sorption isotherms in terms of single CO_2 , N_2 , and CH_4 gases for **2-In** and **NH₂-2-In** were experimentally collected (Figures 3 and S12), respectively. It is

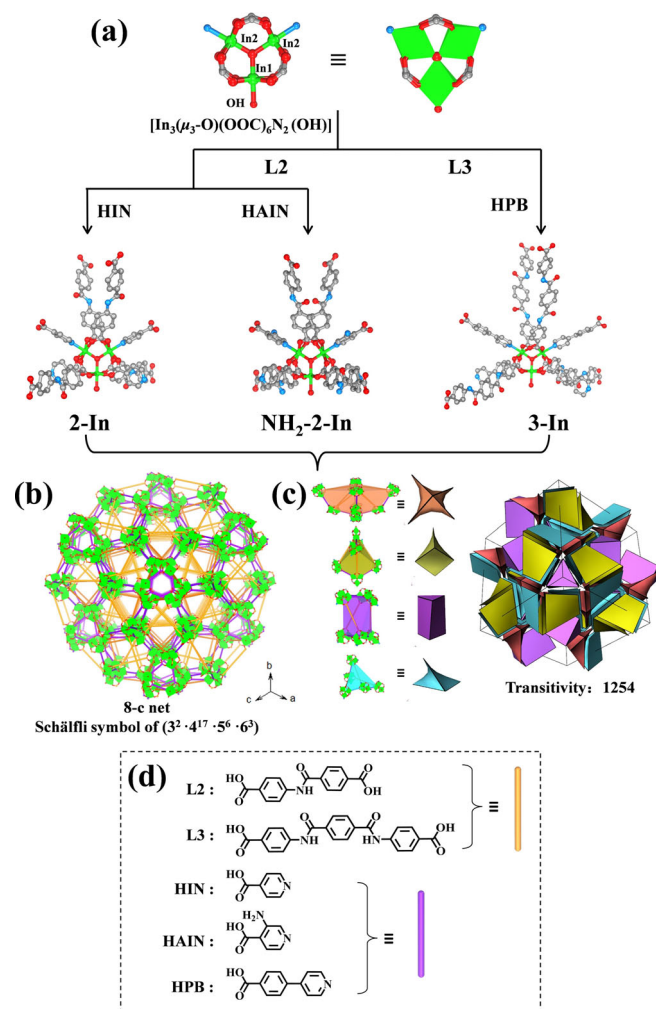


Figure 1. (a) The trinuclear indium cluster and molecular building fragments of **2-In**, **NH₂-2-In** and **3-In**. (b) Structural sketch of the three 8-connected trinuclear indium-based AFMOFs. (c) Four different shapes of pores (left) and the tiling graph of the structures. (d) Structural formula and simplified diagram of ligands. Hydrogen atoms are omitted for clarity. N sky blue, O red, C grey, In green.

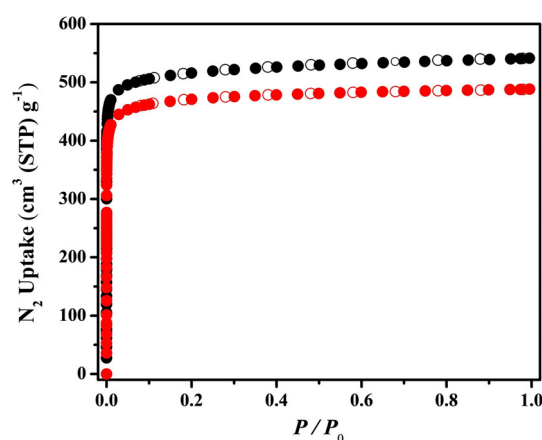


Figure 2. N_2 sorption isotherms at 77 K for **2-In** (black) and **NH₂-2-In** (red) (filled and open symbols represent adsorption and desorption data, respectively).

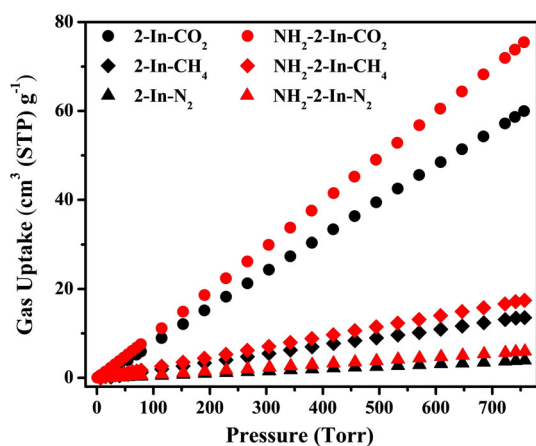


Figure 3. Low-pressure CO₂, N₂, and CH₄ adsorption isotherms at 298 K and 760 torr for **2-In** and **NH₂-2-In**, respectively.

found that both MOFs exhibit relatively high CO₂ uptakes of 60.0 and 75.5 cm³g⁻¹, in contrast to N₂ uptakes of 3.9 and 5.9 cm³g⁻¹, and CH₄ uptakes of 13.5 and 17.5 cm³g⁻¹ at 298 K and 760 torr, respectively. It is obvious that the CO₂ uptakes for **NH₂-2-In** are higher than that for **2-In**, indicating that the dual-functional groups in **NH₂-2-In** certainly increase the affinity between MOF framework-CO₂, consequently leading to higher CO₂ adsorption capability in spite of its reduced apparent surface area and pore volume. The stronger interactions between MOF framework-CO₂ for **NH₂-2-In** were further verified by the slightly higher isosteric heat of CO₂ adsorption (Q_{st}), that is, 18–21 kJ mol⁻¹ in comparison with that of **2-In**, 15–17 kJ mol⁻¹ (Figure S13).

The high porosity and high CO₂ uptakes of both AFMOFs prompted us to investigate their CO₂ capture capability, which is typically evaluated by the two-pairs mixed gases of CO₂/N₂ and CO₂/CH₄, representing two potential applications for post-combustion CO₂ capture and natural gas upgrading, respectively. Consequently, the CO₂ adsorption selectivities for both materials were calculated via the well-defined approach of Ideal Adsorbed Solution Theory (IAST). As shown in Figure S14 and Table S1, the dual-site Langmuir-Freundlich model was applied and found to be best ($R^2 > 0.9998$). The resulting selectivities for CO₂/N₂ (20:80) and CO₂/CH₄ (50:50) mixtures for both MOFs are presented in Table 2 and Figure 4 as a function of the total bulk pressure. The CO₂/N₂ and CO₂/CH₄ selectivities are 10.18 and 12.43, 4.20 and 4.23 for **2-In** and **NH₂-2-In**, respectively. The obvious CO₂ selectivity over N₂ and CH₄ is consistent with above high CO₂ adsorption capability for **2-In** and **NH₂-2-In**.

MOFs	S_{BET} [m ² g ⁻¹]	Q_{st} [kJ mol ⁻¹]	CO ₂ /N ₂ [0.2 bar] IAST/ BT ^[a]	CO ₂ /CH ₄ [0.5 bar] IAST/ BT
2-In	2080	17.09	10.18/9.00	4.20/2.18
NH₂-2-In	1902	20.83	12.43/11.30	4.23/2.26

^[a] BT is representing Breakthrough.

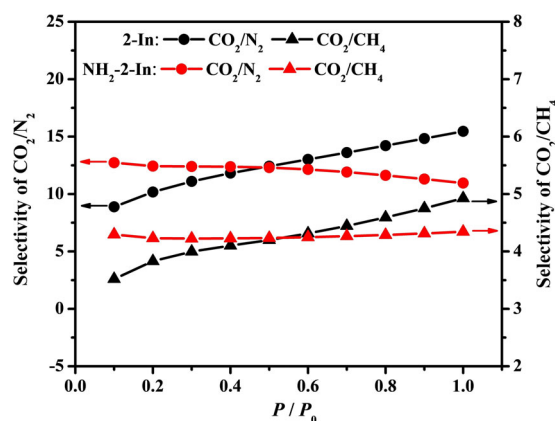


Figure 4. IAST calculated selectivity toward CO₂/N₂ (20:80) and CO₂/CH₄ (50:50) in **2-In** (black) and **NH₂-2-In** (red), respectively.

To evaluate the practical application of both materials toward carbon capture, the transient breakthrough experiments were performed by utilization of the homemade gas separation setup. As seen in Figure 5, the resulting breakthrough curves clearly confirmed the fact that CO₂ was retained in a period of time, while N₂ or CH₄ passed through unencumbered under the mixture of CO₂/N₂ (20:80) and CO₂/CH₄ (50:50) at 298 K and 1 bar. The calculated CO₂ adsorption selectivities from these dynamic breakthrough experiments are basically consistent with the IAST results, demonstrating the promising application of both new AFMOFs toward carbon capture.

Methane storage investigation.

The recent research shows that the fine-tuning series of isorecticular **nbo**-AFMOFs could enhance the methane storage capability, which encourages us to investigate the methane storage performance of both new materials. Therefore, high-pressure excess adsorption isotherms were collected at 273 K and 298 K, respectively, and then empirically transformed to total adsorption isotherms (Figure 6 and Figure S15). The total methane uptake of **2-In** and **NH₂-2-In** reaches 137 and 94 cm³g⁻¹ at 80 bar at 298 K, respectively. The dual-functionalized **NH₂-2-In** exhibits 43 cm³g⁻¹ lower methane uptake compared with that of single amide-functionalized **2-In**, which indicates the high porosity dominates the methane storage capability rather than functionality between both AFMOF materials. Meanwhile, the modest methane storage performances for both MOFs are also probably attributed to their lower surface areas (<3000 m²g⁻¹), improper cage/pore sizes (ideal sizes of 4, 8 or 11 Å). It is worth noting that the CH₄ Q_{st} at zero coverage for both materials are 12.8 and 16.6 kJ mol⁻¹, respectively (Figure S16), which is beneficial for improving the methane storage working capability.

Conclusions

In summary, a new eight-connected isorecticular AFMOF platform based on trinuclear indium has been deliberately de-

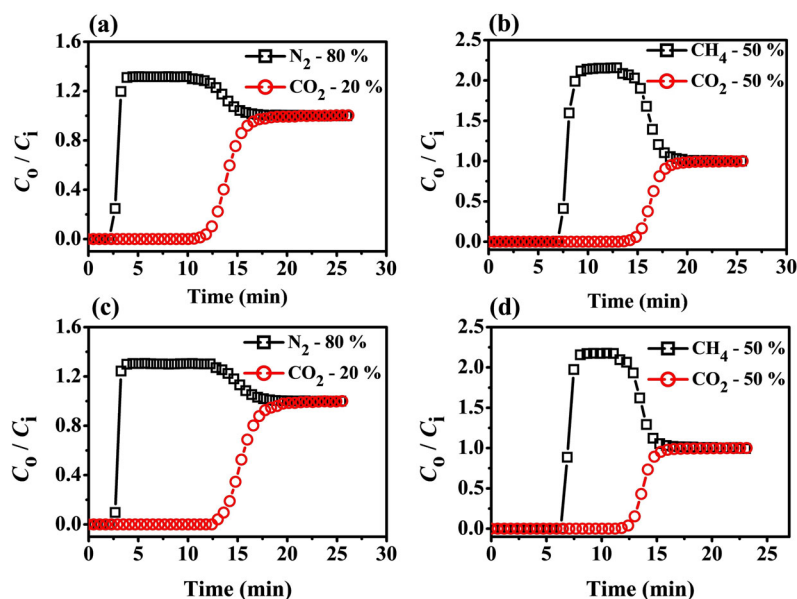


Figure 5. Experimental breakthrough curves for the mixture of CO₂/N₂ (20:80) and CO₂/CH₄ (50:50) in packed columns with 2-In (a, b) and NH₂-2-In (c, d) at 298 K and 1 bar.

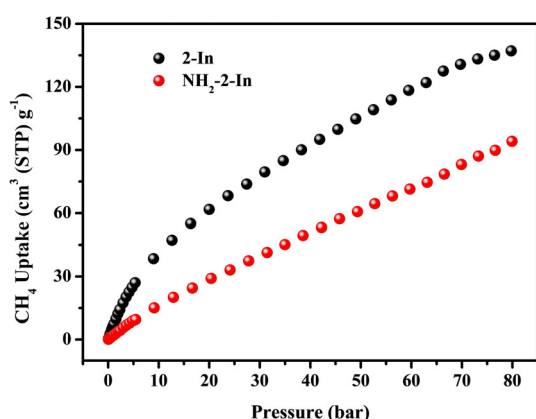


Figure 6. Total methane adsorption isotherms under high-pressure for 2-In (black) and NH₂-2-In (red) at 298 K, respectively.

signed and successfully constructed. These isoreticular AFMOFs exhibit not only multi-functionality and high porosity but also an appreciable carbon capture capacity and a modest amount of methane storage. These results extend the scope of AFMOF inventory and may further facilitate optimization of multivariate MOFs toward high performance in the post-combustion carbon capture and the purification of natural gas.

Experimental Section

1. Materials and Methods.

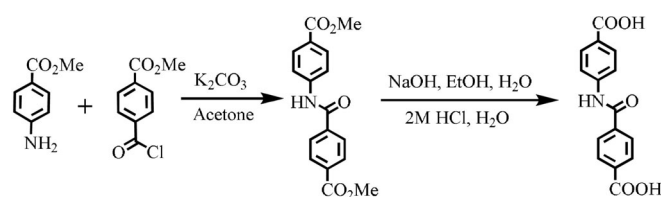
All reagents were obtained from commercial sources and used without further purification. The ligands of H₂L2 and H₂L3 were prepared according to the previously reported procedure with slight modification and the details of synthesis are given in the

supporting information.^[17,18] Fourier-transform infrared (FT-IR) spectrum (4000-400 cm⁻¹, KBr pellet) was collected in the solid state on a Bruker Tensor 27 FT-IR spectrometer. PXRD measurements were performed on a Rigaku MiniFlex 600 diffractometer with CuK α ($\lambda = 1.5406 \text{ \AA}$), and the X-ray tube was operated at 40 kV and 15 mA. High resolution thermogravimetric analysis (TGA) were performed under a continuous N₂ flow and recorded on a Q600SDT thermal analyzer.

2. Synthesis of Materials.

2.1. Ligand syntheses.

Synthesis of organic linker H₂L2.

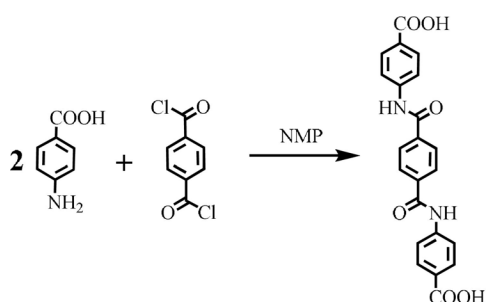


Methyl 4-Aminobenzoate (3.00 g, 19.9 mmol, 1 equiv) and potassium carbonate (6.86 g, 49.7 mmol) were dissolved in 90 mL acetone with stirring. Methyl 4-(chloroformyl)benzoate (3.94 g, 19.9 mmol, 1 equiv) was dissolved separately in 30 mL acetone by sonication and added drop-wise to the stirring reaction mixture. The reaction mixture was sealed and allowed to stir overnight, after which a white solid was collected by filtration. The solid was stirred with water and collected by filtration. The white solid was then suspended in 250 mL THF and hot filtered. The THF filtrate was then subject to rotary evaporation yielding a white solid. The white solid was stirred with hexane, collected by filtration and dried under vacuum, to obtain methyl 4-((4-(methoxycarbonyl)phenyl)amino)benzoate. ¹H NMR (400 MHz, [D₆]DMSO, 25 °C): $\delta = 10.75$ (s, 1H,

CONH), 8.09 (dd, 4H, ArH), 7.96 (dd, 4H, ArH), 3.90 (s, 3H, CH₃), 3.84 ppm (s, 3H, CH₃).

A solution containing methyl 4-(4-(methoxycarbonyl)benzamido)benzoate (4.37 g, 13.9 mmol), NaOH (1.13 g, 28.3 mmol), ethanol (125 mL) and H₂O (125 mL) was prepared and subject to reflux overnight. The resulting transparent solution was cooled to room temperature and acidified with a 75 mL 2 M HCl/ 75 mL H₂O mixture, forming a white suspension. The reaction mixture was sealed and allowed to stir for 3 hours. The product was collected by filtration and washed copiously with water until washings were neutral. The white powder was added to a sample vial which was dried under vacuum, to obtain 4-(4-carboxybenzamido)benzoic acid (H₂L2). ¹H NMR (400 MHz, [D₆]DMSO, 25 °C): δ = 13.04 (s, 2H, COOH), 10.70 (s, 1H, CONH), 8.07 (dd, 4H, ArH), 7.94 ppm (dd, 4H, ArH).

Synthesis of organic linker H₂L3.



Solid 4-aminobenzoic acid (1.15 g, 8.37 mmol) was dissolved in NMP (15 mL) and cooled to 5 °C in ice bath. The solid terephthaloyl chloride (0.812 g, 4.00 mmol) was added slowly for 1 h and the reaction mixture was stirred at 5 °C for 2 h followed by continue stirring at room temperature for an additional 12 h. After that, 20 mL of distilled water was added. The product was filtered and washed with 20 mL of NMP, five times with 50 mL of distilled water, twice with 20 mL of methanol and finally dried at 65 °C for 12 h to obtain 4,4'-(terephthaloylbis(azanediyl))dibenzoic acid (H₂L3). ¹H NMR (400 MHz, [D₆]DMSO, 25 °C): δ = 12.77 (s, 2H, COOH), 10.66 (s, 2H, CONH), 8.10 (s, 4H, ArH), 7.93 ppm (dd, 8H, ArH).

2.2. Preparation of 2-In, NH₂-2-In and 3-In.

[(In₃O)(OH)(L2)₂(IN)₂](solv)_x (**2-In**)

In(NO₃)₃·4.5 H₂O (76.4 mg, 0.2 mmol), H₂L2 (28.5 mg, 0.1 mmol) and HIN (22.14 mg, 0.18 mmol) were mixed in the solvent of 5.5 mL of N,N'-dimethylformamide. The mixture was sealed in a 20 mL scintillation vial and heated to 358 K for 48 h and cooled to room temperature. The colorless polyhedron crystals obtained were collected and washed with DMF. FT-IR: $\tilde{\nu}$ = 3490(m), 3306(w), 2930(m), 2866(w), 1668(s), 1530(m), 1387(s), 1321(m), 1254(m), 1177(m), 1095(m), 1016(w), 866(w), 783(m), 694(w), 661(w), 538(w), 452 cm⁻¹ (w).

[(In₃O)(OH)(L2)₂(AIN)₂](solv)_x (**NH₂-2-In**)

In(NO₃)₃·4.5 H₂O (76.4 mg, 0.2 mmol), H₂L2 (42.75 mg, 0.15 mmol) and HAIN (34.5 mg, 0.25 mmol) were mixed in the solvent of 4.5 mL of N,N'-dimethylformamide. The mixture was sealed in a 20 mL scintillation vial and heated to 358 K for 48 h and cooled to room temperature. The brown polyhedron crystals obtained were collected and washed with DMF. FT-IR: $\tilde{\nu}$ = 3437(m), 3312(w),

2930(m), 2866(w), 1666(s), 1602(w), 1526(m), 1390(s), 1323(m), 1253(m), 1180(m), 1097(m), 1016(w), 865(w), 784(m), 734(w), 662(w), 536(w), 449 cm⁻¹ (w).

[(In₃O)(OH)(L3)₂(PB)₂](solv)_x (**3-In**)

In(NO₃)₃·4.5 H₂O (76.4 mg, 0.2 mmol), H₂L3 (36.36 mg, 0.09 mmol) and HPB (35.82 mg, 0.18 mmol) were mixed in the solvent of 5.0 mL of N,N'-dimethylformamide. The mixture was sealed in a 20 mL scintillation vial and heated to 388 K for 48 h and cooled to room temperature. The colorless polyhedron crystals obtained were collected and washed with DMF. FT-IR: $\tilde{\nu}$ = 3472(m), 2936(m), 2866(w), 1668(s), 1528 (m), 1390(s), 1256(m), 1097(m), 866(w), 785(m), 662(w), 476 cm⁻¹ (w).

3. Single-crystal X-ray structure determination.

Single-crystal X-ray diffraction data were collected on a Bruker D8 venture diffractometer at 153 K using graphite monochromated Cu_{Kα} radiation (λ = 1.5418 Å). Indexing was performed using APEX3 (Difference Vectors method). Data integration and reduction were performed using SaintPlus 6.01. Absorption correction was performed by multi-scan method implemented in SADABS. Space groups were determined using XPREP implemented in APEX3. The structures were solved by direct methods and refined with full-matrix least squares technique using the SHELXTL package.^[19] Non-hydrogen atoms were refined with anisotropic displacement parameters during the final cycles. Hydrogen atoms were located at geometrically calculated positions to their carrier atoms and refined with isotropic thermal parameters included in the final stage of the refinement.

A summary of the crystallographic data are given in Table 1. CCDC 1910435 (**2-In**), 1910436 (**NH₂-2-In**) and 1910437 (**3-In**) contain the supplementary crystallographic data for this paper. These data can be obtained free of charge from The Cambridge Crystallographic Data Centre.

4. Gas sorption measurements.

4.1. Sample activation.

The as-synthesized samples of **2-In** were soaked in acetone for 3 days with acetone refreshing every 8 hours. **NH₂-2-In** was soaked in acetone for 90 min with acetone refreshing every 30 min, and afterwards, the samples were soaked in *n*-hexane for 90 min with *n*-hexane refreshing every 30 min. Then, the Acetone-exchanged sample of **2-In** was activated under vacuum at 303 K for 12 hours, the *n*-hexane-exchanged sample of **NH₂-2-In** was activated under vacuum at 303 K for 4 hours and 323 K for 8 hours.

4.2. Low-pressure adsorption.

Low pressure gas adsorption studies were conducted on a fully automated micropore gas analyzer Autosorb-iQ3 (Quantachrome Instruments) at relative pressures up to 1 atm. The cryogenic temperature was controlled using liquid nitrogen at 77 K. The bath temperature for the CO₂, N₂ and CH₄ sorption measurements was controlled using a recirculating bath containing an ethylene glycol/H₂O mixture. The apparent surface areas were determined from the nitrogen adsorption isotherms collected at 77 K by applying the BET models. Pore size analyses were performed using a cylindrical/spherical NLDFT pore model system by assuming an oxidic (zeolitic) surface.

4.3. Isotheric Heat of Adsorption.

The isotheric heat of adsorption represents the strength of the interactions between adsorbate molecules and the adsorbent lattice atoms and can be used as a measurement of the energetic heterogeneity of a solid surface. The isotheric heat of adsorption at a given amount can be calculated by the Clausius-Clapeyron equation as

$$Q_{st} = -RT^2 \left(\frac{\partial \ln P}{\partial T} \right) n_a$$

where Q_{st} is the isotheric heat of adsorption (kJ mol^{-1}), P is the pressure (kPa), T is the temperature, R is the gas constant, and n_a is the adsorption amount (mmol g^{-1}).

5. IAST calculation.

IAST (Ideal Adsorption Solution Theory)^[20] was used to predict binary mixture adsorption from the experimental pure gas isotherms. In order to perform the integrations required by IAST, the single-component isotherms should be fitted by a proper model. In practice, several methods to do this are available. We found for this set of data that the dual-site Langmuir-Freundlich equation was successful in fitting the data. As can be seen in Table S1, the model fits the isotherms very well ($R^2 > 0.9998$).

$$q = \frac{q_{m,1} b_1 p^{1/n_1}}{1 + b_1 p^{1/n_1}} + \frac{q_{m,2} b_2 p^{1/n_2}}{1 + b_2 p^{1/n_2}}$$

Here, P is the pressure of the bulk gas at equilibrium with the adsorbed phase (kPa), q is the adsorbed amount per mass of adsorbent (mmol g^{-1}), $q_{m,1}$ and $q_{m,2}$ are the saturation capacities of sites 1 and 2 (mmol g^{-1}), b_1 and b_2 are the affinity coefficients of sites 1 and 2 ($1/\text{kPa}^{-1}$), and n_1 and n_2 represent the deviations from an ideal homogeneous surface. The fitted parameters were then used to predict multi-component adsorption with IAST.

The selectivity $S_{A/B}$ in a binary mixture of components A and B is defined as $(x_A/y_A)/(x_B/y_B)$, where x_i and y_i are the mole fractions of component i ($i = A, B$) in the adsorbed and bulk phases, respectively.

The dual-site Langmuir-Freundlich parameters for CO_2 , N_2 , and CH_4 isotherms at 298 K are given in Table S1.

6. Breakthrough experiments.

Breakthrough system used in this study is the homemade HP-MC41 gas separation test system (Nanjing Hope Analytical Equipment Co., Ltd). The flow rates of all gases are regulated by mass flow controllers, and the effluent gas stream from the column is monitored by a gas chromatography (GC). In a typical experiment, ≈ 500 mg of porous sorbent was ground and packed into a stainless-steel column (12 cm length \times 0.30 cm internal diameter) with silica wool filling the void space. The sorbent was activated in situ in the column before the temperature of the column was decreased to 298 K. The packed column was initially purged with helium gas for 30 min until no other gases were detected in the effluent. Then, dry gas mixture of CO_2 - N_2 flow at 2 mL min^{-1} (20:80, v/v) and CO_2 - CH_4 flow at 2 mL min^{-1} (50:50, v/v) were dosed into the column. The dead time was determined using the same column after adsorption saturation. The absolute adsorbed amount of gas i (q_i) is calculated from the breakthrough curve by the equation according literature with modification:^[21]

$$q_i = \frac{F_i \times t_0 V_{\text{dead}} - \int_0^{t_0} F_e \Delta t}{m}$$

Where F_i is the influent flow rate of the specific gas (mL min^{-1}); t_0 is the adsorption time (min); V_{dead} is the dead volume of the system (cm^3); F_e is the effluent flow rate of the specific gas ($\text{cm}^3 \text{ min}^{-1}$); and m is the mass of the sorbent (g). The selectivity of the breakthrough experiment is defined as

$$\alpha = (q_1 / y_1) / (q_2 / y_2)$$

Where y_i is the molar fraction of gas i in the gas mixture. The same breakthrough experiments were repeated three times after the adsorbent saturated with CO_2 was regenerated by a pure He flow.

7. High-pressure adsorption.

High-pressure excess methane adsorption isotherms in the range of 0–80 bar were measured with an automatic volumetric sorption apparatus (BELSORP-HP). The measurement temperatures were controlled by a computer-controlled glycol-water bath. Ultra-high-purity He was used to determine the dead space of the sample cell. The adsorption data were corrected to give the final gravimetric excess adsorption isotherm $n_{ex}(P, T)$, by subtracting the background adsorption measured with the empty sample cell using the same test parameters, shown in Figure S17. The total adsorption, which represents the real gas-storage performance of the porous material but cannot be directly measured, was calculated by [Eq. (1)]:

$$n_{tot}(P, T) = n_{ex}(P, T) + \rho_{\text{gas}}(P, T) \times V_p$$

Where $\rho_{\text{gas}}(P, T)$ is the density of bulk methane at pressure P and temperature T , and V_p is the pore volume of the porous material determined from N_2 adsorption isotherm at 77 K. The volumetric isotherms were obtained by multiplying the gravimetric isotherms with the crystallography density of the host framework.^[22]

Acknowledgements

This work was financially supported by the National Natural Science Foundation of China (No. 21771121 and 21871170), Cheung Kong Scholars Program and the Hundred/Thousand Talents Programs of Shaanxi Province. The authors are grateful to Prof. Yunfeng Zhao for helpful discussions about the breakthrough experiment.

Conflict of interest

The authors declare no conflict of interest.

Keywords: carbon capture · methane storage · metal-organic frameworks · trinuclear indium

- [1] a) M. Eddaoudi, J. Kim, N. L. Rosi, D. T. Vodak, J. Wachter, M. O'Keeffe, O. M. Yaghi, *Science* **2002**, 295, 469–472; b) H. Hayashi, A. P. Côté, H. Furukawa, M. O'Keeffe, O. M. Yaghi, *Nat. Mater.* **2007**, 6, 501–506; c) R. Banerjee, A. Phan, B. Wang, C. Knobler, H. Furukawa, M. O'Keeffe, O. M. Yaghi, *Science* **2008**, 319, 939–943; d) A. Phan, C. J. Doonan, F. J. Uribe-Romo, C. B. Knobler, M. O'Keeffe, O. M. Yaghi, *Acc. Chem. Res.* **2010**, 43, 58–67; e) P. L. Llewellyn, S. Bourrelly, C. Serre, Y. Filinchuk, G. Férey,

- Angew. Chem. Int. Ed.* **2006**, *45*, 7751–7754; *Angew. Chem.* **2006**, *118*, 7915–7918; f) D.-X. Xue, Y. Belmabkhout, O. Shekhah, H. Jiang, K. Adil, A. J. Cairns, M. Eddaoudi, *J. Am. Chem. Soc.* **2015**, *137*, 5034–5040; g) D.-X. Xue, A. J. Cairns, Y. Belmabkhout, L. Wojtas, Y. Liu, M. H. Alkordi, M. Eddaoudi, *J. Am. Chem. Soc.* **2013**, *135*, 7660–7667.
- [2] a) S. M. Cohen, *Chem. Rev.* **2012**, *112*, 970–1000; b) K. K. Tanabe, S. M. Cohen, *Chem. Soc. Rev.* **2011**, *40*, 498–519; c) S. M. Cohen, *Chem. Sci.* **2010**, *1*, 32–36; d) Z.-Q. Wang, S. M. Cohen, *Chem. Soc. Rev.* **2009**, *38*, 1315–1329; e) O. Karagiari, W. Bury, J. E. Mondloch, J. T. Hupp, O. K. Farha, *Angew. Chem. Int. Ed.* **2014**, *53*, 4530–4540; *Angew. Chem.* **2014**, *126*, 4618–4628; f) P. Deria, W. Bury, J. T. Hupp, O. K. Farha, *Chem. Commun.* **2014**, *50*, 1965–1968; g) S. Takaishi, E. J. DeMarco, M. J. Pellin, O. K. Farha, J. T. Hupp, *Chem. Sci.* **2013**, *4*, 1509–1513; h) P. Deria, J. E. Mondloch, E. Tylanakis, P. Ghosh, W. Bury, R. Q. Snurr, J. T. Hupp, O. K. Farha, *J. Am. Chem. Soc.* **2013**, *135*, 16801–16804; i) J. D. Evans, C. J. Sumbly, C. J. Doonan, *Chem. Soc. Rev.* **2014**, *43*, 5933–5951.
- [3] a) D.-X. Xue, Q. Wang, J. Bai, *Coord. Chem. Rev.* **2019**, *378*, 2–16; b) X. Lin, N. R. Champness, M. Schröder, *Top. Curr. Chem.* **2009**, *293*, 35–76; c) W. Yang, A. Greenaway, X. Lin, R. Matsuda, A. J. Blake, C. Wilson, W. Lewis, P. Hubberstey, S. Kitagawa, N. R. Champness, M. Schröder, *J. Am. Chem. Soc.* **2010**, *132*, 14457–14469; d) C. Tan, S. Yang, N. R. Champness, X. Lin, A. J. Blake, W. Lewis, M. Schröder, *Chem. Commun.* **2011**, *47*, 4487–4489; e) S. Yang, X. Lin, W. Lewis, M. Suyetin, E. Bichoutskaia, J. E. Parker, C. C. Tang, D. R. Allan, P. J. Rizkallah, P. Hubberstey, N. R. Champness, K. M. Thomas, A. J. Blake, M. Schröder, *Nat. Mater.* **2012**, *11*, 710–716; f) J. Lü, C. Perez-Krap, M. Suyetin, N. H. Alsmail, Y. Yan, S. Yang, W. Lewis, E. Bichoutskaia, C. C. Tang, A. J. Blake, R. Cao, M. Schröder, *J. Am. Chem. Soc.* **2014**, *136*, 12828–12831; g) S. Yang, A. J. Ramirez-Cuesta, R. Newby, V. Garcia-Sakai, P. Manuel, S. K. Callear, S. I. Campbell, C. C. Tang, M. Schröder, *Nat. Chem.* **2015**, *7*, 121–129.
- [4] a) R. Sun, Y.-Z. Li, J. Bai, Y. Pan, *Cryst. Growth Des.* **2007**, *7*, 890–894; b) R. Sun, S. Wang, H. Xing, J. Bai, Y. Li, Y. Pan, X. You, *Inorg. Chem.* **2007**, *46*, 8451–8453; c) Z. Lu, H. Xing, R. Sun, J. Bai, B. Zheng, Y. Li, *Cryst. Growth Des.* **2012**, *12*, 1081–1084; d) B. Zheng, J. Bai, J. Duan, L. Wojtas, M. J. Zaworotko, *J. Am. Chem. Soc.* **2011**, *133*, 748–751; e) J. Duan, J. Bai, B. Zheng, Y. Li, W. Ren, *Chem. Commun.* **2011**, *47*, 2556–2558; f) J. Duan, Z. Yang, J. Bai, B. Zheng, Y. Li, S. Li, *Chem. Commun.* **2012**, *48*, 3058–3060; g) R. Yun, Z. Lu, Y. Pan, X. You, J. Bai, *Angew. Chem. Int. Ed.* **2013**, *52*, 11282–11285; *Angew. Chem.* **2013**, *125*, 11492–11495; h) M. Zhang, B. Li, Y. Li, Q. Wang, W. Zhang, B. Chen, S. Li, Y. Pan, X. You, J. Bai, *Chem. Commun.* **2016**, *52*, 7241–7244; i) Z. Lu, J. Bai, C. Hang, F. Meng, W. Liu, Y. Pan, X. You, *Chem. Eur. J.* **2016**, *22*, 6277–6285; j) M. Zhang, W. Zhou, T. Phan, K. A. Forrest, W. Liu, Y. He, H. Wu, T. Yidirim, B. Chen, B. Space, Y. Pan, M. J. Zaworotko, J. Bai, *Angew. Chem. Int. Ed.* **2017**, *56*, 11426; *Angew. Chem.* **2017**, *129*, 11584–11430.
- [5] a) C. Volkringer, M. Meddouri, T. Loiseau, N. Guillou, J. Marrot, G. Férey, M. Haouas, F. Taulelle, N. Audebrand, M. Latroche, *Inorg. Chem.* **2008**, *47*, 11892–11901; b) L. Wang, L. Zhang, T. Song, C. Li, J. Xu, L. Wang, *Microporous Mesoporous Mater.* **2012**, *155*, 281–286.
- [6] Y. Liu, J. F. Eubank, A. J. Cairns, J. Eckert, V. C. Kravtsov, R. Luebke, M. Eddaoudi, *Angew. Chem. Int. Ed.* **2007**, *46*, 3278–3283; *Angew. Chem.* **2007**, *119*, 3342–3347.
- [7] a) Y. Liu, V. C. Kravtsov, R. Larsen, M. Eddaoudi, *Chem. Commun.* **2006**, 1488–1490; b) M. H. Alkordi, Y. Liu, R. Larsen, J. F. Eubank, M. Eddaoudi, *J. Am. Chem. Soc.* **2008**, *130*, 12639–12641; c) Q. Li, D.-X. Xue, Y.-F. Zhang, Z.-H. Zhang, Z. Gao, J. Bai, *J. Mater. Chem. A* **2017**, *5*, 14182–14189; d) Q. Li, Z.-L. Fan, D.-X. Xue, Y.-F. Zhang, Z.-H. Zhang, Q. Wang, H.-M. Sun, Z. Gao, J. Bai, *J. Mater. Chem. A* **2018**, *6*, 2148–2156.
- [8] a) H. Deng, C. J. Doonan, H. Furukawa, R. B. Ferreira, J. Towne, C. B. Knobler, B. Wang, O. M. Yaghi, *Science* **2010**, *327*, 846–850; b) L. J. Wang, H. Deng, H. Furukawa, F. Gándara, K. E. Cordova, D. Peri, O. M. Yaghi, *Inorg. Chem.* **2014**, *53*, 5881–5883; c) A. Helal, Z. H. Yamani, K. E. Cordova, O. M. Yaghi, *Nat. Sci. Rev.* **2017**, *4*, 296–298.
- [9] a) W. Lu, Z. Wei, Z.-Y. Gu, T.-F. Liu, J. Park, J. Tian, M. Zhang, Q. Zhang, T. Gentle, M. Bosch, H.-C. Zhou, *Chem. Soc. Rev.* **2014**, *43*, 5561–5593; b) A. Kirchon, L. Feng, H. F. Drake, E. A. Joseph, H.-C. Zhou, *Chem. Soc. Rev.* **2018**, *47*, 8611–8638.
- [10] a) H. Deng, S. Grunder, K. E. Cordova, C. Valente, H. Furukawa, M. Hmadeh, F. Gándara, A. C. Whalley, Z. Liu, S. Asahina, H. Kazumori, M. O’Keeffe, O. Terasaki, J. F. Stoddart, O. M. Yaghi, *Science* **2012**, *336*, 1018–1023; b) O. M. Yaghi, *J. Am. Chem. Soc.* **2016**, *138*, 15507–15509; c) B. Rungtaweeworant, C. S. Diercks, M. J. Kalmutzki, O. M. Yaghi, *Faraday Discuss.* **2017**, *201*, 9–45; d) S. J. Lyle, R. W. Flaig, K. E. Cordova, O. M. Yaghi, *J. Chem. Educ.* **2018**, *95*, 1512–1519.
- [11] G. Férey, C. Mellot-Draznieks, C. Serre, F. Millange, J. Dutour, S. Surble, I. Margiolaki, *Science* **2005**, *309*, 2040–2042.
- [12] C. Serre, C. Mellot-Draznieks, S. Surblé, N. Audebrand, Y. Filinchuk, G. Férey, *Science* **2007**, *315*, 1828–1831.
- [13] a) M. Pang, A. J. Cairns, Y. Liu, Y. Belmabkhout, H. C. Zeng, M. Eddaoudi, *J. Am. Chem. Soc.* **2012**, *134*, 13176–13179; b) D. Feng, K. Wang, Z. Wei, Y.-P. Chen, C. M. Simon, R. K. Arvapally, R. L. Martin, M. Bosch, T.-F. Liu, S. Fordham, D. Yuan, M. A. Omary, M. Haranczyk, B. Smit, H.-C. Zhou, *Nat. Commun.* **2014**, *5*, 5723.
- [14] Y.-B. Zhang, W.-X. Zhang, F.-Y. Feng, J.-P. Zhang, X.-M. Chen, *Angew. Chem. Int. Ed.* **2009**, *48*, 5287–5290; *Angew. Chem.* **2009**, *121*, 5391–5394.
- [15] X. Zhao, C. Mao, K. T. Luong, Q. Lin, Q.-G. Zhai, P. Feng, X. Bu, *Angew. Chem. Int. Ed.* **2016**, *55*, 2768–2772; *Angew. Chem.* **2016**, *128*, 2818–2822.
- [16] X. Gu, Z.-H. Lu, Q. Xu, *Chem. Commun.* **2010**, *46*, 7400–7402.
- [17] R. S. Forgan, R. J. Marshall, M. Struckmann, A. B. Bleine, D.-L. Long, M. C. Bernini, D. Fairen-Jimenez, *CrystEngComm* **2015**, *17*, 299–306.
- [18] B. T. Nguyen, H. L. Nguyen, T. C. Nguyen, K. E. Cordova, H. Furukawa, *Chem. Mater.* **2016**, *28*, 6243–6249.
- [19] G. M. Sheldrick, *Acta Crystallogr. Sect. A* **2008**, *64*, 112.
- [20] a) A. L. Myers, J. M. Prausnitz, *AIChE J.* **1965**, *11*, 121; b) Y. S. Bae, K. L. Mulfort, H. Frost, P. Ryan, S. Punnathanam, L. J. Broadbelt, J. T. Hupp, R. Q. Snurr, *Langmuir* **2008**, *24*, 8592–8598; c) B. Mu, F. Li, K. S. Walton, *Chem. Commun.* **2009**, 2493–2495.
- [21] Y. Zhao, K. X. Yao, B. Teng, T. Zhang, Y. Han, *Energy Environ. Sci.* **2013**, *6*, 3684–3692.
- [22] J.-M. Lin, C.-T. He, Y. Liu, P.-Q. Liao, D.-D. Zhou, J.-P. Zhang, X.-M. Chen, *Angew. Chem. Int. Ed.* **2016**, *55*, 4674–4678; *Angew. Chem.* **2016**, *128*, 4752–4756.

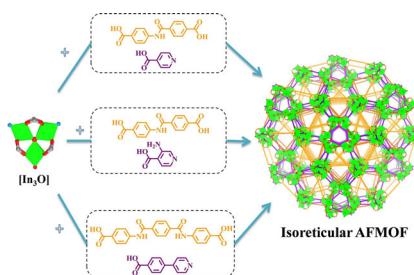
Manuscript received: April 23, 2019

Revised manuscript received: May 22, 2019

Version of record online: ■ ■ ■ 0000

FULL PAPER

By means of reticular chemistry, three isorecticular eight-connected trinuclear indium-based amide-functionalized metal–organic frameworks were deliberately designed and successfully constructed. They exhibit not only multifunctionality and high porosity but also an appreciable carbon capture capacity and a modest amount of methane storage.



Zong-Hui Zhang, Qian Wang,
Dong-Xu Xue,* Junfeng Bai*



Syntheses, Structures and Sorption Properties of Three Isorecticular Trinuclear Indium-Based Amide-Functionalized Metal–Organic Frameworks

